Single molecule visualization of native centromeric nucleosome formation reveals coordinated deposition by kinetochore proteins and centromere DNA sequence

Andrew R. Popchock[a], Joshua D. Larson[b], Julien Dubrulle[c], Charles L. Asbury[b], Sue Biggins [a,1]

[a] Howard Hughes Medical Institute, Basic Sciences Division, Fred Hutchinson Cancer Center, Seattle, WA 98109, USA
[b] Department of Physiology and Biophysics, University of Washington, Seattle, WA, USA
[c] Shared Resources, Fred Hutchinson Cancer Center, Seattle, WA 98109, USA
[1] Correspondence: sbiggins@fredhutch.org

Abstract

Eukaryotic chromosome segregation requires the kinetochore, a conserved megadalton-sized machine that forms on specialized centromeric chromatin containing CENP-A, a histone H3 variant. CENP-A deposition requires a conserved chaperone protein HJURP that targets it to the centromere, but it has remained unclear whether HJURP has additional functions beyond CENP-A targeting and why high AT DNA content, which disfavors nucleosome assembly, is widely conserved at centromeres. To overcome the difficulties of studying nucleosome formation in vivo, we developed a microscopy assay that enables direct observation of de novo centromeric nucleosome recruitment and maintenance at single molecule resolution. Using this assay, we discover that CENP-A can arrive at centromeres without its chaperone, but stable incorporation depends on HJURP and on DNA-binding proteins of the inner kinetochore. We also show that homopolymer AT runs in the yeast centromeres are essential for efficient CENP-A deposition. Together, our findings reveal requirements for stable nucleosome formation and provide a foundation for further studies of the assembly and dynamics of native kinetochore complexes.

Keywords: Centromeric nucleosome, CENP-A, HJURP, Ndc10, Centromere, CoSMoS, Kinetochore, Chromosome segregation, TIRF microscopy

Introduction

Replicated chromosomes must be accurately segregated to opposite poles during mitosis, a process that relies on their attachment to mitotic spindle microtubules via a conserved megadalton-sized protein network called the kinetochore [3-7]. Errors in this process can lead to the rapid accumulation of mis-segregated chromosomes resulting in a cellular condition called aneuploidy, a hallmark of cancerous cells [8-11]. To ensure the fidelity of this process, kinetochores are assembled each cell cycle onto defined regions of chromosomes called centromeres [12-14]. Among different organisms, centromeres vary in size and architecture and are epigenetically defined by the recruitment of a specialized H3 histone variant called CENP-A [15, 16]. The centromere-specific targeting and deposition of CENP-A relies upon an essential conserved chaperone protein, HJURP [17-21]. Once established, this specialized CENP-A nucleosome is then recognized by specific kinetochore proteins that enable complete kinetochore complex formation [22]. CENP-A deposition onto centromeres is tightly regulated in cells as ectopic mis-incorporation contributes to chromosomal instability (CIN) [23]. Consistent with this, CENP-A and HJURP overexpression, which can be driven by p53 loss [24], are common among various cancer types and have emerged as therapeutic cancer targets because higher levels are correlated with poor prognosis [25].

Centromeric nucleosomes are critical for chromosome segregation, so it is surprising that the only widely conserved feature of centromeric DNA, its AT-rich content, is canonically a poor template for nucleosome assembly [26, 27]. Assembling centromeric histones with centromeric DNA *in vitro* results in intrinsically unstable nucleosomes, making it difficult to study the functional role of the AT-rich centromeric DNA [28-30]. Recent breakthrough structural studies of CENP-A nucleosomes assembled with native centromeric DNA have found a more loosely associated centromeric DNA-nucleosome complex, which may provide distinct binding sites for the recruitment of DNA-binding kinetochore proteins [31, 32]. However, these reconstitutions required the use of a single-chain antibody fragment (scFv) to stabilize the nucleosome in both yeast and human reconstitutions [31, 32]. More complex reconstitutions that included additional kinetochore proteins required modification of the centromeric DNA sequence to include the histone targeting sequence Widom 601 DNA [31, 33-35], underscoring the difficulty of reconstituting stable kinetochore structures on centromeric DNA. While a more complete reconstitution of the constitutively centromere associated network (CCAN) kinetochore proteins assembled onto a CENP-A nucleosome was achieved on α-satellite DNA, the functional role of AT-rich centromeric DNA remains unclear [36].

In contrast to most eukaryotes, budding yeast have sequence-specific point centromeres consisting of similar but not identical ~125 bp DNA segments containing three different centromere-defining elements, CDEI, CDEII and CDEIII [3, 37, 38]. CDEI and CDEIII have consensus sites to recruit the centromere binding factors 1 and 3 (Cbf1 and CBF3), respectively. One function of Cbf1 is to protect centromeres from transcription to ensure chromosome stability [39, 40], while the CBF3 complex (consisting of Ctf3, Cep3, Skp1 and Ndc10) coordinates with the Cse4 (CENP-A in humans) specific chaperone Scm3 (HJURP in humans) to promote the deposition of $Cse4^{CENP-A}$ at CDEII [17, 31, 41, 42]. Similar to other organisms, the CDEII element lacks sequence homology but consists of highly AT-rich DNA [31]. Changes in the length or AT-content of CDEII compromise centromere stability *in vivo* [12, 43, 44]. More recently, the presence of homopolymeric runs of A and T within the CDEII elements were identified to play a significant role in centromere function *in vivo* [45], but the underlying mechanism driven by these homopolymeric runs remains unknown due to the inherent instability of these nucleosomes *in vitro* [28-30]. One possibility is that these sequences play a role in exclusion of the canonical H3 nucleosome, as H3 eviction has been proposed as a potential function of centromeres [29, 46]. Due to their difficulty to study in cells, it remains unclear why these CDEII centromere sequences are essential *in vivo* yet are such poor templates for nucleosome formation and kinetochore assembly *in vitro.*
To resolve this paradox between the requirements for centromere sequence in nucleosome formation *in vitro* versus *in vivo,* it is imperative

to determine what additional factors stabilize centromeric nucleosomes in a physiological context. Recent structural reconstitutions that contain a Cse4^{CENP-A} nucleosome in complex with additional inner kinetochore proteins [31], including all the components of the CCAN (which comprise the network of inner kinetochore proteins that remain associated with Cse4^{CENP-A} throughout the cell cycle [1]), have highlighted significant interaction between centromeric DNA and inner kinetochore proteins around the nucleosome [1, 31]. These reconstitutions have provided insight into potential candidate factors, yet the use of non-native centromeric DNA may limit model testing. Ideally, interrogation of nucleosome formation in cells is needed but doing so is extremely challenging, not only because the CENs *in vivo* are too close to be resolved individually in light microscopy, but also because they remain fully occupied for most of the cell cycle [47, 48].

To address these limitations, we developed a new technique utilizing **T**otal **I**nternal **R**eflection **F**luorescent **M**icroscopy (TIRFM) to enable direct observation of centromeric nucleosome formation at a single molecule resolution. This technique was inspired by the "colocalization single molecule spectroscopy" (CoSMoS) technique [49-51], adapting it to spread individual centromere DNAs out spatially to enable the observation of formation of Cse4^{CENP-A} nucleosomes on centromeric DNA in real time. We adapted this technique to interrogate the role of centromeric DNA and more broadly assess native centromeric nucleosome complex formation. To achieve this resolution, *Saccharomyces cerevisiae* was used as a model system due to their simplified and sequence-defined point centromeres that contain only a single Cse4^{CENP-A} nucleosome [42, 52]. Under these conditions, stable recruitment of Cse4^{CENP-A} was highly specific and dependent upon native centromere sequence, recapitulating *in vivo* requirements for nucleosome formation. Through continuous visualization of individual centromeres, we observed unexpectedly dynamic association of Cse4^{CENP-}individual centromeres: specifically, we found that Cse4^{CENP-A} deposition occurred in two distinct steps: first, a "targeting" step, consisting of a reversible binding of Cse4^{CENP-A} for which Scm3^{HJURP} was dispensable, followed by a second "stabilization" step, for which Scm3^{HJURP} and DNA-binding inner kinetochore proteins were required. Stabilization was blocked by constraining both ends of the centromeric DNA template, suggesting that it also requires DNA wrapping by Cse4^{CENP-A}. Stabilization was also significantly influenced by both the sequence composition of the CDEII element and the subsequent coordination of inner kinetochore proteins during kinetochore assembly. Together, these findings shed new light on the mechanisms that catalyze formation of a robust centromeric DNA-based platform for kinetochore assembly and provide a foundation to address additional steps in the kinetochore assembly process.

Results

Efficient recruitment of Cse4^{CENP-A} to individual centromeric DNAs.

To study the requirements and dynamics of centromeric nucleosome assembly, we adapted a recently developed method for bulk assembly of yeast kinetochores *de novo* in cell extracts [53], modifying it for single molecule imaging via TIRFM. Template DNAs consisting of the chromosome III centromere (117 bp), with ~70 bp of pericentromeric DNA plus ~250 bp of linker DNA on each side (referred to as 'CEN3 DNA'), were linked to a streptavidin-functionalized coverslip surface [54] through a biotin tag (Figure 1A). A dye-label added to the free end of the DNA allowed its visualization. Introducing whole cell extracts prepared from strains with fluorescent kinetochore proteins into the chamber enabled recruitment and retention of the labeled kinetochore proteins on individual CEN3 DNA molecules to be monitored for colocalization via CoSMoS. Initially, we performed simple endpoint analyses, where the cell lysate after incubation for 90 min with surface-linked CEN3 DNAs was washed from the chamber and colocalization was then measured from individual images. We refer to such measurements as "endpoint colocalization assays", to distinguish them from the continuous time-lapse measurements described later.

We first tested whether Cse4^{CENP-A} and the CBF3 complex, which is required for Cse4^{CENP-A} targeting, were specifically recruited to CEN3 DNA molecules. We made lysates from cells expressing endogenously tagged Ndc10-mCherry, which binds to CEN3 DNA as part of the CBF3 complex, and Cse4^{CENP-A}-GFP (Figure 1B). It was previously shown that the position of the GFP tag in Cse4 affects protein function, so we used an internal Cse4 tag that is fully functional [55]. Both these labeled proteins showed high endpoint colocalization (Figure 1C), with ~70% or ~50% of the CEN DNA molecules associating with Ndc10 or Cse4, respectively (Figure 1D). To ensure this colocalization was specific, we tested a mutant CEN3 DNA template (CDEIII^{mut}) with two substitutions that prevent CBF3 complex binding [53, 56]. As expected, endpoint colocalization of Ndc10-mCherry on this mutant template was nearly abolished (Supp. Figure 1A, B). Because CBF3c binding is required for Cse4^{CENP-A} nucleosome formation at CEN3 DNA, it abrogates subsequent kinetochore assembly [53, 57]. Thus, colocalization of Cse4^{CENP-A} with the CDEIII^{mut} DNA template was also nearly abolished (Supp. Figure 1C, D). To confirm that the recruitment of Cse4^{CENP-A} to CEN3 DNA depends on the known requirements *in vivo*, we utilized proteasomal degradation of its chaperone Scm3^{HJURP} [53, 58] and confirmed that Cse4^{CENP-A} no longer colocalizes to CEN3 DNA [53] (Supp. Figure 1C, D). To further probe the fidelity of the assay, we quantified the stoichiometry of Ndc10 and Cse4^{CENP-A} via photobleaching assays. When photobleaching was performed on Ndc10-mCherry associated with CEN3 DNA, it photobleached predominantly in two steps (Supp. Figure 1E, F) with a photobleaching step distribution similar to other previously characterized dimeric proteins [59, 60]. This is consistent with structural studies that show that Ndc10 is a homodimer within the CBF3 complex [31, 55, 57, 61] and with the range reported *in vivo* [48]. Photobleaching analysis of Cse4^{CENP-A} associated with CEN3 DNA yielded similar results, with the majority of Cse4^{CENP-A}-GFP photobleaching in two steps (Supp. Figure 1G, H). This dimeric stoichiometry is similar to nucleosome reconstitutions [17, 31] as well as fluorescence and photobleaching analysis of Cse4^{CENP-A} at centromeres *in vivo* [48, 62]. Taken together, these results suggest that the copy numbers of both Ndc10 and Cse4^{CENP-A} within extract kinetochore assemblies are consistent with *in vivo* estimates.

Cse4^{CENP-A} binds more stably to the centromere when preceded by CBF3 complex component Ndc10.

We next set out to monitor the dynamics of Cse4^{CENP-A} centromere targeting by performing continuous time-lapse TIRFM of CEN3 DNA for colocalization. Ndc10 binds to the conserved chaperone Scm3^{HJURP} to target Cse4^{CENP-A} to centromeres [17, 21] and has been proposed to promote DNA bending to initiate Cse4^{CENP-A} nucleosome formation [1] [17]. We labeled Ndc10 with an mCherry fluorescent protein to allow its simultaneous detection in a separate color channel from GFP-labeled Cse4^{CENP-A} (Figure 2A). To assist in analysis of colocalization events taking place on hundreds of CEN3 templates simultaneously, we developed an automated analysis software package in MATLAB (see Methods). Briefly, identification of CEN3 DNAs was followed by identification of colocalization events in both protein channels at each CEN3 DNA to determine colocalization residence times and lengths (Figure 2B), termed "residence lifetime assays". This analysis enabled the rapid quantification of many independent colocalization events within a single field of view over a single imaging sequence for comparison.

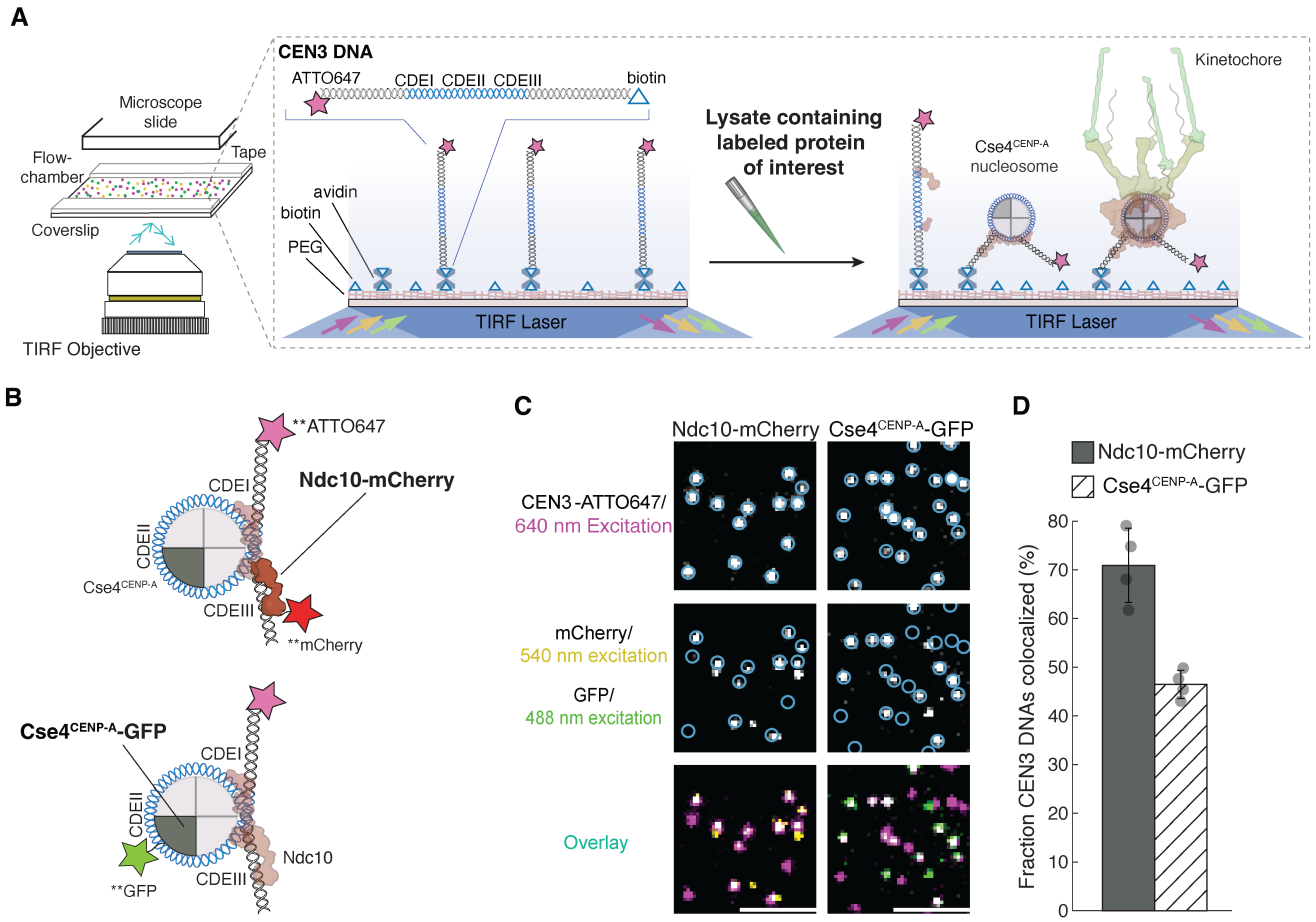

Figure 1. Ndc10 and Cse4^{CENP-A} assemble with high efficiency onto CEN3 DNAs in extract. (**A**) Schematic of the TIRFM colocalization assay. Yeast lysate containing a fluorescent protein(s) of interest is added to a coverslip with immobilized fluorescent CEN3 DNA. After incubation, the lysate is washed from the chamber and the CEN3 DNA and fluorescent kinetochore proteins are imaged via TIRFM. (**B**) Schematic of fluorescent label locations around the centromeric nucleosome used in (C) for colocalization imaging. (**C**) Example images of TIRFM endpoint colocalization assays. Top panels show CEN3 DNA (blue circles) that was incubated with Ndc10-mCherry (top-left panel) or Cse4^{CENP-A}-GFP (top-right) lysates. Middle panels show the Ndc10-mCherry (middle-left panel) and Cse4^{CENP-A}-GFP (middle-right) in relation to blue DNA circles. Bottom panels show an overlay of the DNA channel (magenta) with Ndc10-mCherry (yellow, bottom-left panel) and Cse4^{CENP-A}-GFP (green, bottom-right). (**D**) Quantification of observed endpoint colocalization of Ndc10 (71.0 ± 7.6%, avg ± s.d. n=4 experiments, each examining ~1,000 DNA molecules from different extracts), and Cse4^{CENP-A} (46.5 ± 2.9%, avg ± s.d. n=4 experiments, each examining ~1,000 DNA molecules from different extracts). Scale bars 3 µm.

Using this analysis, we simultaneously identified residence lifetimes for both Ndc10 and Cse4^{CENP-A} throughout a 45 min TIRFM time-lapse acquisition (Figure 2C, Supp. Figure 2A). We then analyzed the residence lifetimes via Kaplan-Meyer analysis and found that Cse4^{CENP-A} had a much shorter median lifetime (approximately half) than Ndc10 (Figure 2D), which was unexpected because both proteins appear stably bound to the centromere outside of S-phase replication, with slow turnover kinetics *in vivo* [55, 63]. Photo-stability estimates of the endogenous fluorophores used in colocalization lifetime analysis assays revealed that the residence lifetimes of Ndc10 (Supp. Figure 2B) were more severely limited by photobleaching than Cse4^{CENP-A} (Supp. Figure 2C) but did not truncate the majority of Cse4^{CENP-A} residence lifetimes. To ensure that Cse4^{CENP-A} behavior was not a consequence of a particular CEN sequence, we confirmed similar Cse4^{CENP-A} recruitment and colocalizations on several CEN3 templates from different chromosomes (Supp. Figure 3). It should be noted that genetic backgrounds where Cse4^{CENP-A} and a partner protein were fluorescently tagged (either Ndc10 or its chaperone Scm3^{HJURP}- as was the case in Supp. Figure 3) resulted in reduced Cse4^{CENP-A} localization to CEN DNA likely due to mild genetic interactions between tagged proteins, but this did not prevent residence lifetime analysis via TIRFM time-lapse experiments. Taken together these data suggest that Cse4^{CENP-A} is more dynamic than Ndc10 at centromeres prior to its stable incorporation.

To further dissect behavioral differences between Ndc10 and Cse4^{CENP-A}, we identified instances where a residence of Cse4^{CENP-A} coincided with a Ndc10 residence on the same CEN3 DNA, termed "ternary residence" (Figure 2B). All identified Cse4^{CENP-A} ternary residences with Ndc10 were then pooled and separated from all Cse4^{CENP-A} residences that occurred on CEN3 alone (Figure 2C). When Kaplan-Meyer analysis of these two subpopulation residence lifetimes was performed, ternary Cse4^{CENP-A} residences that occurred with both CEN3 DNA and Ndc10 remained associated with CEN3 DNA for significantly longer durations (Figure 2E). Additionally, when all observed colocalization pulses were organized by time of initiation, we found that in ternary Cse4^{CENP-A} residences, CEN3 DNA association of Ndc10 preceded Cse4^{CENP-A} the vast majority of the time (Figure 2F, G). These observations are consistent with *in vivo* findings where it has been established that Ndc10 is required for Scm3^{HJURP}-dependent and thought to coordinate with the Cbf1 complex to promote nucleosome formation [41].

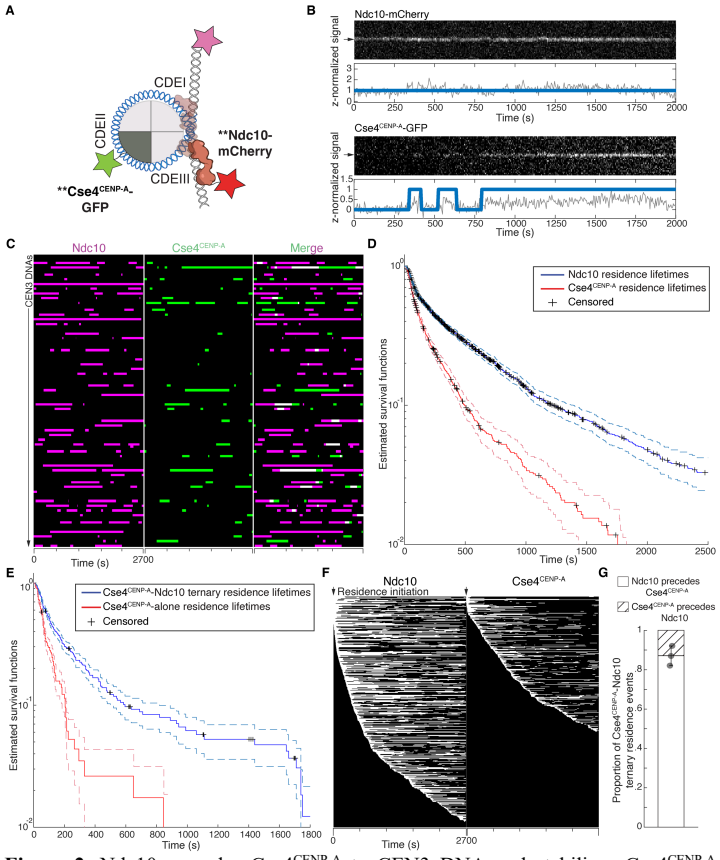

Figure 2. Ndc10 precedes Cse4^{CENP-A} to CEN3 DNA and stabilizes Cse4^{CENP-A} residence on CEN3 DNA. (**A**) Schematic of fluorescent label locations around the centromeric nucleosome used for colocalization imaging. (**B**) Representative residence lifetime assay traces of Ndc10 (top) and Cse4^{CENP-A} (bottom) on a single CEN3 DNA. Top panel includes kymograph of Ndc10 (top-568 nm) in relation to single identified CEN3 DNA (arrow), with normalized intensity trace (grey-bottom) as well as identified colocalization residences (blue). Bottom panel includes kymograph of Cse4^{CENP-A} (top-488 nm) in relation to the same identified CEN3 DNA (arrow), with normalized intensity trace (grey-bottom) as well as identified colocalization residences (blue). Instances where Ndc10 and Cse4^{CENP-A} residence coincides represent simultaneous observation of both proteins on single CEN3 DNA, termed ternary residence. Images were acquired every 5 seconds with normalized fluorescence intensity shown in arbitrary units. (**C**) Example graph of total identified colocalization residences observed on CEN3 DNA per imaging sequence. Each row represents one identified CEN3 DNA with all identified residences shown over entire imaging sequence (2700 s) for Ndc10 (magenta) and Cse4^{CENP-A} (green) with merge indicating ternary residences (white). Complete series shown in Supp. Figure 2A. (**D**) Kaplan Meyer analysis of CEN3 DNA residence lifetimes of Ndc10 (blue – median lifetime of 195 s, n=2481 over 3 experiments of ~1000 DNA molecules using different extracts) and Cse4^{CENP-A} (red – median lifetime of 96 s, n=1377 over 3 experiments of ~1000 DNA molecules using different extracts). 95% confidence intervals indicated (dashed lines). (**E**) Cse4^{CENP-A} residence time is higher if colocalized together with Ndc10. Kaplan Meyer analysis of ternary residence lifetimes of Cse4^{CENP-A} and Ndc10 on a CEN3 DNA molecule (blue – median lifetime of 109 s, n=750 over 3 experiments of ~1000 DNA molecules using different extracts) and residence lifetimes of Cse4^{CENP-A} alone (red – median lifetime of 52 s, n=348 over 3 experiments of ~1000 DNA molecules using different extracts). Ternary residences include simultaneous Ndc10 residence at any point during continuous Cse4^{CENP-A} residence on CEN3 DNA. 95% confidence intervals indicated (dashed lines). (**F**) Example plot of total identified residences observed on CEN3 DNA per imaging sequence of Ndc10 (left) and Cse4^{CENP-A} (right) independently sorted by residence initiation time, starting at the top with initiation time of 0 s (arrow). (**G**) Quantification of all observed Ndc10 and Cse4^{CENP-A} ternary residence events where proportion when Ndc10 precedes Cse4^{CENP-A} is 0.87 ± .05 and Cse4^{CENP-A} precedes Ndc10 is 0.13 ± .05 (avg ± s.d., n=653 over 3 experiments of ~1000 DNA molecules using different extracts).

The conserved chaperone Scm3^{HJURP} is a limiting cofactor that promotes stable association Cse4^{CENP-A} with the centromere.

In our initial analysis of Cse4^{CENP-A} colocalization, we noticed a biphasic behavior, consisting of many short colocalizations (<120 s) with less common longer colocalizations (>300 s), that could not be fully correlated to Ndc10 occupancy on CEN3 DNA, as many short associations of Cse4^{CENP-A} occur on CEN3 DNAs associated with Ndc10 (Figure 2C). To interrogate this behavior, we simultaneously visualized Cse4^{CENP-A} and the essential conserved chaperone protein Scm3^{HJURP}, which exhibits DNA-binding activity and is required for centromere targeting and Cse4^{CENP-A} maintenance in cells [17, 21], via continuous time-lapse TIRFM imaging (Figure 3A). Residence lifetime assays revealed shorter Scm3^{HJURP} residence times on CEN3 DNA than Cse4^{CENP-A} (Figure 3A, B). This difference was confirmed in residence lifetime analysis (Supp. Figure 4), consistent with its shorter turnover rates *in vivo* [55]. Strikingly, when ternary residences of Cse4^{CENP-A} with Scm3^{HJURP} on CEN3 DNA were pooled and separated from residences of Cse4^{CENP-A} on CEN3 DNA alone, the largest subpopulation were those Cse4^{CENP-A} residences in the absence of Scm3^{HJURP} association (Figure 3B, C). This was unexpected because Scm3^{HJURP} is required for Cse4^{CENP-A} deposition to centromeres *in vivo* [17, 21].

We next assayed whether the two distinct Cse4^{CENP-A} residence subpopulations, those that formed ternary associations with its chaperone and those that did not, behave differently on CEN3 DNA. Analysis of the residence lifetimes of the two subpopulations revealed that ternary Cse4^{CENP-A}-Scm3^{HJURP} residences remained bound to CEN3 DNA for significantly longer durations than those Cse4^{CENP-A} residences with CEN3 DNA in the absence of Scm3^{HJURP} (Figure 3D). This result suggests that Scm3^{HJURP} helps promote more stable binding of Cse4^{CENP-A} despite its relatively rare co-occupancy at CEN3 DNA. This observation led us to modify the availability of this complex *in vivo* to assess resulting changes in Cse4^{CENP-A} behavior. The E3 ubiquitin ligase Psh1 and chaperone Scm3^{HJURP} directly compete for Cse4^{CENP-A} binding [64], so we reasoned that we could reduce the amount of Cse4^{CENP-A}-Scm3^{HJURP} complex levels in cells by Psh1 overexpression and, conversely, that the amount of Cse4^{CENP-A}- Scm3^{HJURP} complex could be increased by Scm3^{HJURP} overexpression. We introduced an ectopic copy of either Psh1 or Scm3^{HJURP} under an inducible *GAL* promoter into cells containing labeled Cse4^{CENP-A} and Scm3^{HJURP}. Inducing short pulses of either protein did not significantly alter the total levels of Cse4^{CENP-A} in whole cell extracts (Supp. Figure 5A), so we performed endpoint colocalization analysis to quantify the total level of stable Cse4^{CENP-A} colocalization at CEN3 DNA after incubation. Short pulsed Scm3^{HJURP} overexpression led to a significant increase in Cse4^{CENP-A} levels at CEN3 DNA, while overexpression of Psh1 had the opposite effect (Supp. Figure 5B, C) indicating that Scm3 levels were limiting for Cse4 deposition. Residence lifetime analysis of Cse4^{CENP-A} confirmed that the median lifetime was significantly increased when Scm3^{HJURP} was overexpressed and significantly decreased when Psh1 was overexpressed (Supp. Figure 5D). These lifetime changes correlated with the propensity for Cse4^{CENP-A} to form ternary residences with Scm3^{HJURP} on CEN3 DNA (Supp. Figure 5E), suggesting they reflect changes in the availability of the Cse4^{CENP-A}-Scm3^{HJURP} complex. To assess if these perturbations to Cse4^{CENP-A} were consequential in cells, we grew cells under constant induction and found significant growth phenotypes when this complex was limited (Supp. Figure 5F). These data indicate that Scm3^{HJURP} is limiting for stable centromeric nucleosome formation in our single molecule assembly assay and suggest that availability of the Cse4^{CENP-A}-Scm3^{HJURP} complex is likewise important for cell viability.

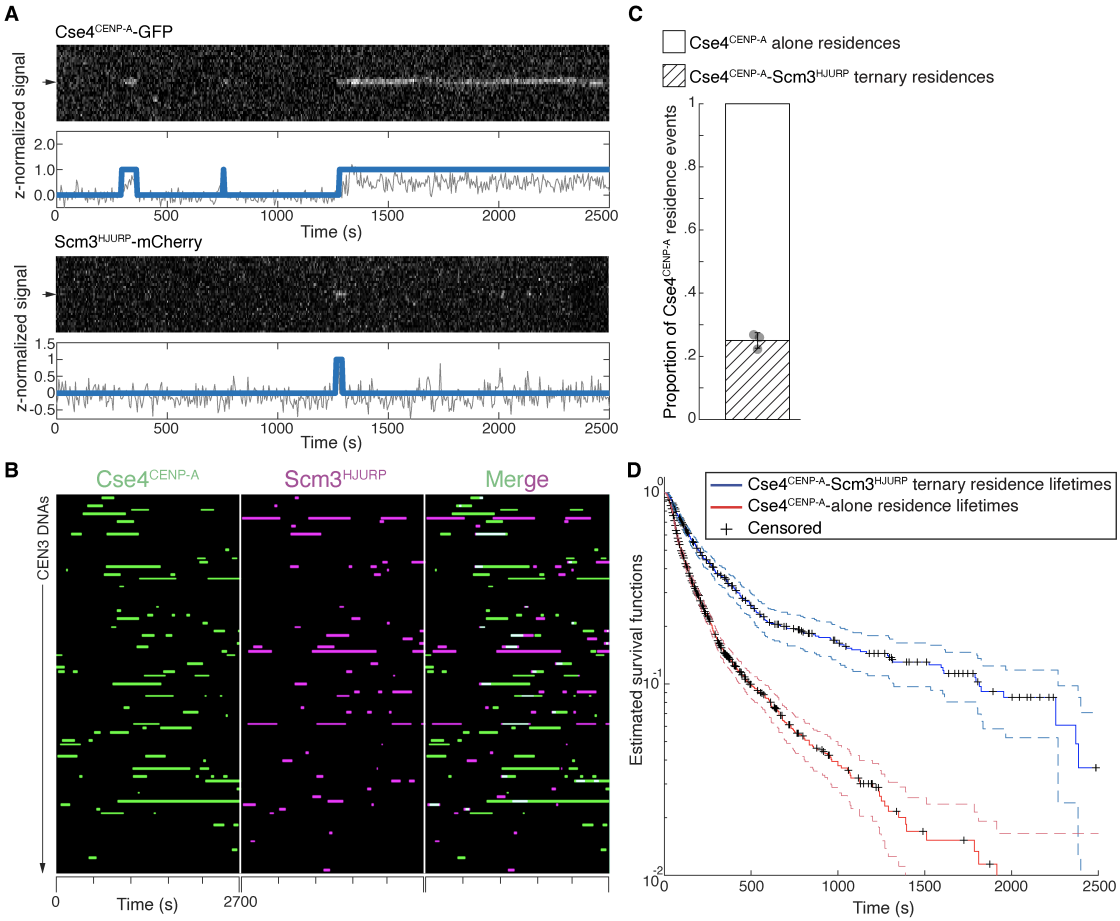

Figure 3. Residence of Cse4^{CENP-A} on centromeric DNA is increased in the presence of its chaperone Scm3^{HJURP}. (**A**) Representative residence lifetime assay traces of Cse4^{CENP-A} (top) and Scm3^{HJURP} (bottom) on a single CEN3 DNA. Top panel includes kymograph of Cse4^{CENP-A} (top-488 nm) in relation to single identified CEN3 DNA (arrow), with normalized intensity trace (grey-bottom) as well as identified residences (blue). Bottom panel includes kymograph of Cse4^{CENP-A} (bottom-568 nm) in relation to the same identified CEN3 DNA (arrow), with normalized intensity trace (grey-bottom) as well as identified residences (blue). Cases where Scm3^{HJURP} and Cse4^{CENP-A} residence coincides represent simultaneous observation of both proteins on single CEN3 DNA, termed ternary residence. Images acquired every 5 seconds with normalized fluorescence intensity shown in arbitrary units. (**B**) Example plot of total identified residences observed on CEN3 DNA per imaging sequence. Each row represents one identified CEN3 DNA with all identified residences shown over entire imaging sequence (2700 s) for Cse4^{CENP-A} (green) and Scm3^{HJURP} (magenta) with merge indicating ternary residences (white). Complete plot shown in Supp. Figure 4A. (**C**) Quantification of the proportion of Cse4^{CENP-A} and Scm3^{HJURP} ternary residences with CEN3 DNA compared to CEN3 DNA residences of Cse4^{CENP-A} alone (0.25 ± .02 and 0.75 ± .02 respectively, avg ± s.d. n=1904 over 3 experiments of ~1000 DNA molecules using different extracts). Ternary residences include simultaneous Scm3^{HJURP} residence at any point during continuous Cse4^{CENP-A} residence on CEN3 DNA. (**D**) Longer residence lifetimes are measured for Cse4^{CENP-A} that include Scm3^{HJURP}. Kaplan Meyer analysis of ternary residence lifetimes of Cse4^{CENP-A} and Scm3^{HJURP} on CEN3 DNA (blue – median lifetime of 195 s, n=510 over 3 experiments of ~1000 DNA molecules using different extracts) and residences on CEN3 DNA of Cse4^{CENP-A} alone (red - of 94 s (n=1832 over 3 experiments of ~1000 DNA molecules using different extracts). 95% confidence intervals indicated (dashed lines).

Stable Cse4^{CENP-A} association is blocked when centromere DNA templates are tethered at both ends.

Our observation of two subpopulations of Cse4^{CENP-A} molecules on CEN3 DNAs, including brief binders and longer-residing molecules that correlated with Scm3^{HJURP}, suggest a two-stage process for Cse4^{CENP-A} deposition that begins with transient, chaperone-independent targeting and is followed by chaperone-dependent stabilization. We hypothesized that the transition to more stable Cse4^{CENP-A} binding might require wrapping of the CEN DNA around the Cse4^{CENP-A}-containing histone octamer. If wrapping were indeed required for stabilization, then restricting the ability of the DNA to adopt a wrapped configuration should inhibit stabilization. To test this prediction, we created CEN3 DNA templates with biotins at both ends to enable double-ended attachment to the coverslip surface. Tethering both ends of the template should limit its ability to twist or shorten, and thus to encircle a Cse4^{CENP-A} histone octamer, properties which are proposed to be a consequence of Cse4^{CENP-A} nucleosome formation at centromere [65, 66].

Double tethering of DNA templates was done by introduction of an additional biotin handle in place of an organic dye to a shortened version (250bp) of the CEN3 DNA to allow both ends of the CEN3 template to be tethered to the coverslip surface simultaneously (Figure 4A). We first tested for a nucleosome-protected DNA fragment using a bulk assembly assay. We performed assembly assays using a shortened 250 bp single-tethered CEN3 template, the double-tethered template or a shortened 250bp CDEIII^{mut} template DNA functionalized to streptavidin-coated magnetic beads as done previously [53]. The assemblies were then subjected to mild micrococcal nuclease (MNase) digestion, which preferentially cuts the unbound DNA between nucleosomes leaving protected DNA intact. There was strong protection of ~140 bp DNA observed in the single-tether template, presumably due to nucleosome

formation, that was almost completely abrogated when double-tethered (Figure 4B). This lack of protection was also observed with the 250 bp CDEIII^{mut} template DNA that does not stably recruit Cse4^{CENP-A} [53]. Protection of the CEN3 DNA template was driven by Cse4^{CENP-A}-containing nucleosomes because this DNA fails to recruit H3 [53]. These observations suggest that spatial restriction of the template can prevent Cse4 nucleosome assembly.

We next sought to analyze Cse4^{CENP-A} behavior on the double-tethered CEN3 template. Because the double tethered templates lacked an organic dye for visualization, we used Ndc10-mCherry as a fiducial marker for the CEN3 DNAs due to its high colocalization percentage (Figure 1B), rapid arrival, stable colocalization behavior, and our finding that most Cse4^{CENP-A} colocalizations occur after Ndc10 (Figure 2C, E). Endpoint colocalization of Cse4^{CENP-A} was reduced more than 2-fold on the double-

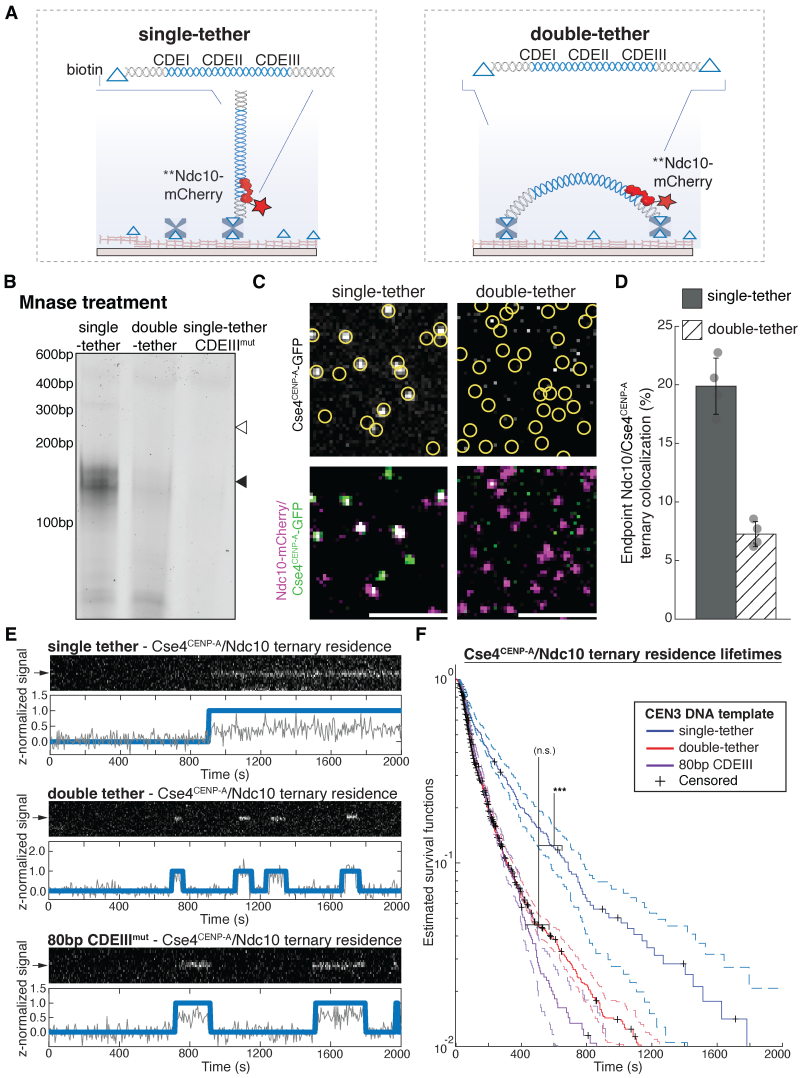

Figure 4. Synthetic restriction of Cse4^{CENP-A} nucleosome formation severely restricts Cse4^{CENP-A} residence lifetimes on CEN3 DNA. (A) Schematic of single vs. double-tether CEN3 DNA TIRFM colocalization assay. (B) DNA from post-assembly Mnase-treated beads that were functionalized with either 250 bp single-tether, 250 bp double-tether or 250 bp CDEIIImut CEN3 DNA was visualized on an agarose gel. Black arrow indicates Cse4^{CENP-A} nucleosome protected DNA (~150 bp); white arrow indicates theoretical location of undigested template DNA (250 bp). (C) Example images of TIRFM endpoint colocalization assays. Top panels show Cse4^{CENP-A}-GFP/Ndc10 ternary colocalizations visualized on single-tethered CEN3 DNA (top-left panel) or on double-tethered CEN3 DNA (top-right panel) with colocalization shown in relation to Ndc10 in yellow circles. Bottom panels show overlay of Ndc10 channel (magenta) with Cse4^{CENP-A}-GFP (green). Scale bars 3 µm. (D) Quantification of observed ternary colocalization of Cse4^{CENP-A} with Ndc10 (right) on single-tethered CEN3 DNA containing Ndc10 (19.9 ± 2.4%, avg ± s.d. n=4 experiments, each examining ~1,000 DNA molecules from different extracts) and on double-tethered CEN3 DNA (7.3 ± 1.1%, avg ± s.d. n=4 experiments, each examining ~1,000 DNA molecules from different extracts). (E) Representative residence lifetime assay traces of ternary Cse4^{CENP-A} residences with Ndc10 on single-tethered CEN3 DNA (top), double-tethered CEN3 DNA (middle) or on 80 bp CDEIII CEN3 DNA (bottom). Each example includes kymographs of Cse4^{CENP-A} (488 nm-top) with normalized intensity trace (grey-bottom) as well as identified residences (blue). Images acquired every 5 seconds with normalized fluorescence intensity shown in arbitrary units. (F) Residence times for Cse4^{CENP-A} on double-tethered CEN3 DNAs are shorter than on single-tethered CEN3 DNAs and equivalent to those on non-functional mutant CEN DNAs. Kaplan Meyer analysis of ternary residences of Cse4^{CENP-A} with Ndc10 on single-tethered CEN3 DNA (blue – median lifetime of 153 s, n=379 over 3 experiments of ~1000 DNA molecules using different extracts) on double-tethered CEN3 DNA (red – median lifetime of 80 sec, n=4647 over 3 experiments of ~1000 DNA molecules using different extracts) and on 80 bp CEN3 DNA (purple – median lifetime of 81 sec, n=1131 over 3 experiments of ~1000 DNA molecules using different extracts). 95% confidence intervals are indicated (dashed lines). No significant difference between double-tethered and 80 bp CEN3 DNA survival plots (n.s.) and significant difference between those two survival plots and single-tether DNA as determined by log-rank test (*** = two tailed p-value >.0001).

tethered CEN3 DNAs relative to single-tethered controls (Figure 4C, D). Likewise, time-lapse experiments revealed that median residence lifetimes for Cse4^{CENP-A} (Figure 4E, F) on double-tethered CEN3 DNAs were significantly shorter than on single-tethered templates (153 s vs. 80 s). Residence times of Cse4^{CENP-A} on single-tethered templates were comparable to those of the previously measured Cse4^{CENP-A}/Ndc10 ternary residence lifetimes (median lifetime of 109 s vs. 153 s, Figure 2D, 4F), but residence times on double-tethered templates were significantly shorter, with lifetimes closer to Cse4^{CENP-A} alone (absence of Scm3^{HJURP}) residence lifetimes (median lifetime of 96 s vs. 80 s, Figure 3D, 4E). The shortened Cse4^{CENP-A} residence times on double-tethered templates were very similar to those on a single-tethered, severely truncated 80-bp template that is too short to form even a single wrap around the Cse4^{CENP-A}-containing core particle (median lifetime of 80 s vs. 81 s, Figure 4D, E, Supp. Figure 6). Thus, physical restriction of the CEN3 DNA template, either by shortening it or limiting its mobility, prevents stable association of Cse4^{CENP-A}, quantitatively reproducing the transient binding seen in the absence of the chaperone protein Scm3^{HJURP}. These observations suggest that stable deposition of Cse4 requires physical wrapping of the CEN DNA around the histone core, that Scm3^{HJURP} has an important role in the wrapping process, and that wrapping of centromeric DNA is a key kinetic hurdle in CEN nucleosome formation.

DNA-binding CCAN elements stabilize the centromeric nucleosome.

Given the inherent instability of bare centromeric nucleosomes *in vitro* [28, 30], we hypothesized that additional stabilization after nucleosome formation might be provided by the binding of centromeric DNA-associated CCAN proteins. Such an additional stabilization step would explain our observations where Cse4^{CENP-A} and Scm3^{HJURP} colocalized together on CEN3 DNA without yielding long-lived (>300 s) Cse4^{CENP-A} association (Figure 3). To test this idea, we identified two conserved CCAN proteins that interact with CEN3 DNA, Chl4^{CENP-N} and Okp1^{CENP-Q}, based on recent structural studies [1, 31]. Chl4^{CENP-N} binds close to the Cse4^{CENP-A} nucleosome and forms a DNA-binding groove that binds the centromere and stabilizes an extended DNA section adjacent to the nucleosome (Figure 5A). Mutation of this Chl4^{CENP-N} DNA-binding groove (*chl4^{K13S}*) exhibits genetic interactions with mutants in Cse4^{CENP-A}, making it an ideal candidate to test its contribution to nucleosome stability [1]. Okp1^{CENP-Q} forms a heterodimer with Ame1^{CENP-U} that has DNA binding activity [67] and has been proposed to interact with an N-terminal extension of Cse4^{CENP-A} within the nucleosome structure [1, 68] (Figure 5A). We therefore assayed Cse4^{CENP-A} endpoint colocalization in *chl4^{K13S}* and *okp1-AID* extracts and found that it was significantly impaired even though total Cse4^{CENP-A} levels in the extracts were not significantly altered (Figure 5B-D). Consistent with previous analysis where lower endpoint Cse4^{CENP-A} colocalization was associated with reduced residence lifetimes (Figure 4C-E), analysis of Cse4^{CENP-A} residence lifetimes in both *chl4^{K13S}* and *okp1-AID* extracts showed the likelihood of Cse4^{CENP-A} to remain stably associated with CEN3 DNA was significantly reduced in both contexts (Figure 5E, F). This disruption in centromeric nucleosome maintenance is consistent with another stabilization step that occurs when additional DNA-binding kinetochore proteins associate after Cse4^{CENP-A} nucleosome formation.

DNA-composition of centromeres contributes to genetic stability through Cse4^{CENP-A} recruitment.

We next sought to investigate the role of centromeric DNA sequence in centromeric nucleosome formation. We reasoned that if centromeric DNA composition functioned beyond simple exclusion of H3 nucleosomes, our TIRFM colocalization assays would be well suited to

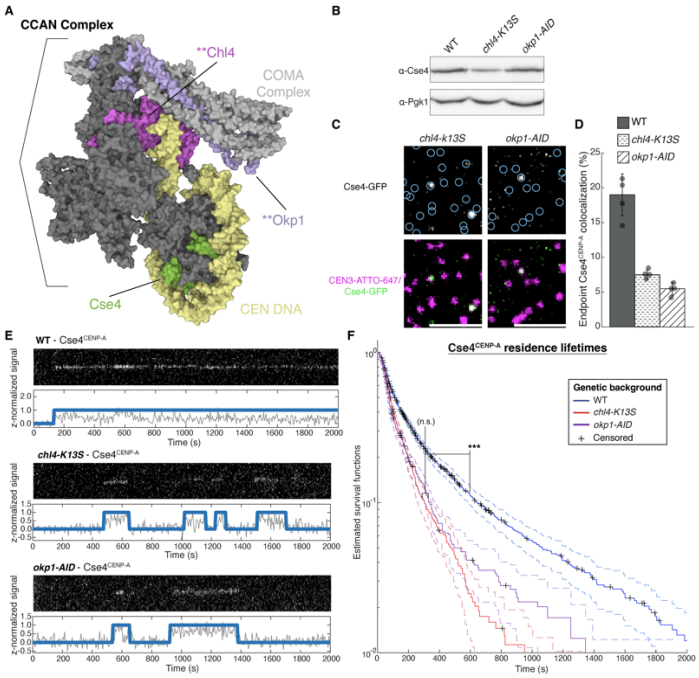

Figure 5. DNA-binding CCAN proteins stabilize the nucleosome to provide a platform for kinetochore assembly. (**A**) Structure of yeast CCAN in complex with Cse4^{CENP-A} with CEN3 DNA (yellow), Cse4^{CENP-A} (green), Chl4^{CENP-N} (magenta) and Okp1^{CENP-Q} (purple), highlighting DNA-adjacent regions targeted by *chl4-K13S* mutant or proteasomal degradation of Okp1^{CENP-Q} (*okp1-AID)*. Image of 6QLD [45] created with Mol* [87]. (**B**) Immunoblot analysis of whole cell extracts from WT, *chl4-K13S* and *okp1-AID* cells using indicated antibodies. (**C**) Example images of TIRFM endpoint colocalization assays. Top panels show visualized Cse4^{CENP-A}-GFP on CEN3 DNA in extracts from *chl4-K13S* (top-left panel) or auxin-treated *okp1-AID* strains (*okp1-AID*, top-right panel) with colocalization shown in relation to identified CEN3 DNA in blue circles. Bottom panels show overlay of CEN3 DNA channel (magenta) with Cse4^{CENP-A}-GFP (green), Scale bars 3 µm. (**D**) Quantification of endpoint colocalization of Cse4^{CENP-A} with CEN3 DNA in extracts from WT, *chl4*-K13S, or *okp1-AID* genetic backgrounds (19.9 ± 2.4%, 7.6 ± 0.7%, 5.4 ± 0.9%, avg ± s.d. n=4 experiments, each examining ~1,000 DNA molecules from different extracts). (**E**) Representative residence traces of Cse4^{CENP-A} signal on CEN3 DNA in WT (top), *chl4-K13S* (middle), or *okp1-AID* (bottom) extracts. Each example includes kymographs of Cse4^{CENP-A} (488 nm-top) with normalized intensity trace (grey-bottom) as well as identified residences (blue). Images acquired every 5 seconds with normalized fluorescence intensity shown in arbitrary units. (**F**) Kaplan Meyer analysis of residence lifetimes of Cse4^{CENP-A} on CEN3 DNA in extracts from WT (blue - median lifetime of 110 s, n=1832 over 3 experiments of ~1000 DNA molecules using different extracts), *chl4-K13S* (red – median lifetime of 80 s, n=744 over 3 experiments of ~1000 DNA molecules using different extracts) and *okp1-AID* (purple – median lifetime of 65 s, n=717 over 3 experiments of ~1000 DNA molecules using different extracts) genetic backgrounds. 95% confidence intervals indicated (dashed lines). Significant difference between Cse4^{CENP-A} in WT lysates compared to those in *chl4-K13S* or *okp1-AID* backgrounds (*** = two-tailed p-value <.0001), which were not significantly different from each other (n.s.) as determined by log-rank test.

test for changes in Cse4^{CENP-A} deposition dynamics. To do this, we took advantage of earlier work that specifically probed the role of CDEII sequence composition on centromere stability *in vivo* [45]. Briefly, CDEII sequences were tested for genetic stability *in vivo* by generating synthetic pools of both genetically stable and unstable CDEII mutants that maintained total AT content but varied in homopolymeric content (A/T-run content defined as an A/T repeat ≥4, Figure 6A). We tested whether the differences in genetic stability correlated with the ability of the templates to retain Cse4^{CENP-A} using endpoint colocalization assays.

While all mutants recruited lower levels of stable Cse4^{CENP-A} compared to the WT CEN3 DNA template, the more stable CDEII mutants recruited higher levels of Cse4^{CENP-A} than their unstable counterparts (Figure 6B, C). To further dissect the contribution of A/T run-content, we monitored the binding behavior of both Cse4^{CENP-A} and Scm3^{HJURP} via residence lifetime analysis. To approximate preference for a particular CEN DNA template, we averaged the total Cse4^{CENP-A} residences in a 45 min imaging sequence to the total CEN DNA templates for each CDEII mutant and found a clear correlation between stability *in vivo* and Cse4^{CENP-A} association (Figure 6D). Although the averaged residences of Scm3^{HJURP} remained consistent across CDEII mutants (Figure 6D), there was a clear correlation between the endpoint colocalization of Cse4^{CENP-A} and the genetic stability of the CDEII mutant centromeres *in vivo* (Figure 6E - inset). When Cse4^{CENP-A} endpoint colocalization was instead plotted against A/T run content, higher Cse4^{CENP-A} endpoint colocalization (and thus higher genetic stability) was correlated to higher CDEII A/T run content (Figure 6E).

To further test this correlation, we generated several other CDEII templates that maintained high AT-sequence composition yet had very little A/T run content. Use of a CDEII mutant that contained a substitution of satellite DNA from human chromosomes (α-sat) failed to recruit stable Cse4^{CENP-A} in endpoint colocalization assays despite its high AT-sequence content (Figure 6E). We next tested the CDEIII hybrid-Widom

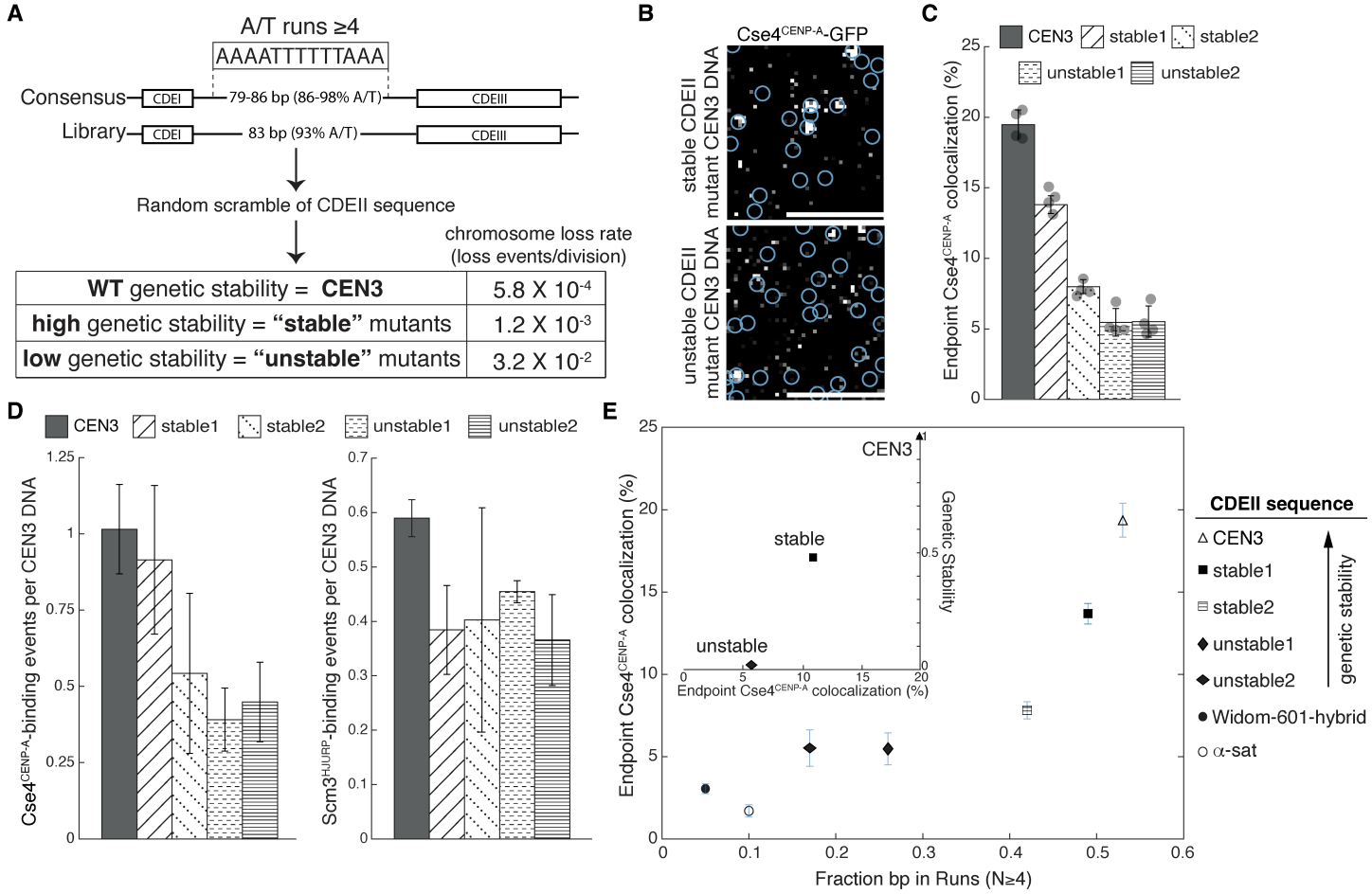

Figure 6. DNA-composition of centromeres contributes to genetic stability through Cse4^{CENP-A} recruitment. (**A**) Overview of CDEII mutants generated for stability assays where overall % of A/T content was maintained while A/T run content was randomly varied and selected for genetic stability (adapted from [43]) including reported chromosome loss rates of WT and CDEII mutant pools [43].(**B**) Example images of TIRFM endpoint colocalization assays. Visualized Cse4^{CENP-A}-GFP on stable1 CDEII-mutant DNA (top panel) or on unstable1 CDEII-mutant DNA (bottom panel) with colocalization shown in relation to identified CEN DNA in blue circles. Scale bars 3 µm. (**C**) Quantification of endpoint colocalization of Cse4^{CENP-A} on CEN3, stable1, stable2, unstable1, and unstable2 CEN DNA (19.9 ± 2.4%, 13.8 ± 0.6%, 7.8 ± 0.5%, 5.5 ± 1.0%, 5.5 ± 1.1%, avg ± s.d. n=4 experiments, each examining ~1,000 DNA molecules from different cell extracts). (**D**) More stable CDEII mutants have higher average Cse4^{CENP-A} binding than their unstable counterparts. Average residences of Cse4^{CENP-A} per CEN DNA (left) on CEN3, stable, stable2, unstable1, and unstable2 CEN DNA (1.02 ± 0.15, 0.92 ± 0.24, 0.54 ± 0.26, 0.39 ± 0.10, 0.45 ± 0.13, avg ± s.e.m. n=3 experiments of ~1000 DNA molecules using different cell extracts) and average residences of Scm3^{HJURP} per CEN DNA (right) on CEN3, stable1, stable2, unstable1, and unstable2 CEN3 DNA (0.59 ± 0.03, 0.38 ± 0.08, 0.40 ± 0.21, 0.46 ± 0.02, 0.37 ± 0.08, avg ± s.e.m. n=3 experiments of ~1000 DNA molecules using different cell extracts). (**E**) Genetic stability of CDEII sequence is directly proportional to stable Cse4^{CENP-A} recruitment, which depends upon CDEII sequence A/T run content. Plot of fraction of all CDEII bp that occur in repeats of 4 or more A or T (fraction bp in runs (N≥4)) in CEN3, stable1, stable2, unstable1, unstable2, Widom-601 hybrid and α-sat CEN DNA (0.53, 0.49, 0.41, 0.26, 0.17, 0.05, 0 .10), versus the observed colocalization of Cse4^{CENP-A} on CEN3, stable1 stable2, unstable1, unstable2, Widom-601 hybrid and α-sat CEN DNA (19.9 ± 2.4%, 13.8 ± 0.6%, 7.8 ± 0.5%, 5.5 ± 1.0%, 5.5 ± 1.1%, 3.1 ± 0.3%, 1.7 ± 0.4% (avg ± s.d. n=4)). Inset plot of endpoint colocalization percentage of Cse4^{CENP-A} on CEN3, stable mutants (average), and unstable mutants (average) (19.9%, 10.8% and 5.5% respectively) versus genetic stability (chromosome loss normalized to CEN3) of WT, stable mutants, and unstable mutants (1.0, 0.48 and 0.02 respectively).

601 hybrid sequence that readily forms centromeric nucleosome in recombinant reconstitutions [1], but it also failed to recruit stable Cse4^{CENP-A} in endpoint colocalization assays (Figure 6E). To ensure that the hybrid-Widom 601 sequence was not saturated by the canonical H3 histone, we also monitored H3 incorporation. We found that the hybrid-Widom 601 DNA incorporated low levels of H3, similar to WT CEN3 DNA, in both bulk assembly assays (Supp. Figure 7A) and endpoint colocalization assays (Supp. Figure 7B). Such low levels of H3 incorporation were somewhat unexpected, as Widom-601 readily forms stable H3 nucleosomes when reconstituted [33], but this may point to differences in *de novo* histone formation that have yet to be fully studied. Removal of the CDEIII sequence from the hybrid-Widom 601 resulted in reversion back to the canonical Widom 601 DNA sequence and yielded an approximately 2-fold increase in H3 incorporation (Supp. Figure 7B). Because the primary difference between the Widom-601 and hybrid-Widom 601 is the binding of the CBF3 complex, this reduction in H3 incorporation may indicate negative regulation of H3 binding by the presence of centromeric DNA-binding kinetochore proteins. Together, these data highlight a critical functional role of the centromeric CDEII element sequence, where conservation of A/T run content within centromeric DNA is essential for centromeric stability through stable recruitment of Cse4^{CENP-A}.

Discussion

Here, we report adaptation of a cell-free system to autonomously assemble native centromeric nucleosomes on centromeric DNA with CoSMos to enable the study of native centromeric nucleosome formation at spatiotemporal resolutions not previously accessible. Continuous monitoring of Cse4^{CENP-A} revealed that several cofactors coordinate at the centromere to promote stable recruitment and maintenance. These cofactors include the DNA-binding CBF3c component Ndc10, as well as the conserved chaperone Scm3^{HJURP}. We found that Scm3^{HJURP} was a limiting cofactor that promoted stable centromeric Cse4^{CENP-A} association but was not required for transient centromere association. This stabilization of Cse4^{CENP-A} likely occurred through catalysis of centromeric DNA wrapping because we observed that synthetic restriction of centromeric DNA wrapping impaired the stable recruitment of Cse4^{CENP-A}. Using recent structural kinetochore reconstitutions as a guide, we were also able to show that once formed, the centromeric nucleosome must be stabilized by DNA-associated kinetochore proteins within the CCAN, highlighting the tight coordination of kinetochore assembly at the inner kinetochore. This finding may in part explain instances where Cse4^{CENP-A} colocalizes to CEN3 DNA with its chaperone Scm3^{HJURP} yet fails to stably associate that were observed in our assays. We presume that in those instances, the Cse4^{CENP-A} nucleosome may have been successfully initiated, but failure of subsequent CCAN kinetochore proteins permitted the dissolution of the nucleosome complex (Figure 7). Using this assay, we were also able to interrogate the CDEII DNA element and identify a role for sequence composition in stable centromeric nucleosome recruitment which correlated to centromere stability in cells. Taken together, this assay enabled the assessment at high resolution of the native nucleosome assembly process on centromeric DNA as well as a functional role of centromere DNA sequence composition.

Formation of a native centromeric nucleosome

Despite over a decade of ongoing study, reconstituting Cse4^{CENP-A} nucleosomes on yeast centromeric DNA has remained remarkably elusive. Recent structural studies have started to shed light on these complexes, yet there are fundamental differences between these reconstitutions and native kinetochore assemblies. One such example is our finding that the Widom 601-hybrid sequence that readily stabilized the Cse4^{CENP-A} nucleosome *in vitro* was a poor template for Cse4^{CENP-A} recruitment and stable nucleosome formation *de novo* (Figure 7D). Structural models using non-native CEN3 DNA required significant rearrangements around the centromeric nucleosome to permit CCAN assembly, including dissociation of the CBF3 complex [1, 31]. However, we did not observe a significant reduction in CBF3 complex colocalization, even after sufficient incubation to allow full *de novo* kinetochore assembly [53]. Our findings are consistent with observed CBF3 behavior in cells [63] and highlight both the potential significant differences between *in vitro* reconstitutions of kinetochore complexes and their native counterparts as well as the significant advantage of assembling kinetochores under native conditions.

Continuous monitoring of Cse4^{CENP-A} nucleosome formation at individual centromere templates revealed an additional function of the chaperone Scm3^{HJURP} at centromeres beyond its canonical centromere targeting role [17, 41]. We found that Scm3^{HJURP} is a limiting kinetochore assembly factor and catalyzes stable Cse4^{CENP-A} recruitment (Figure 3, 4). This suggests that other chaperone proteins that bind to Cse4^{CENP-A} allow for transient centromere interactions that do not lead to nucleosome formation, consistent with reports that Cse4^{CENP-A} binds to chaperones CAF-1, Spt6, and DAXX [69-71]. Because restriction of DNA wrapping of Cse4^{CENP-A} severely limited stable association, Scm3^{HJURP} most likely promotes stable Cse4^{CENP-A} recruitment through catalysis of centromeric DNA wrapping. While several chaperones have been shown to limit ectopic deposition of Cse4^{CENP-A} [70, 72, 73], it is likely that Scm3^{HJURP} promotes specific deposition at centromeres through two non-exclusive mechanisms: (1) tethering of Cse4^{CENP-A} via Scm3^{HJURP}-Ndc10 binding to promote centromeric DNA wrapping or (2) stabilization of a Cse4^{CENP-A}-centromere DNA intermediate through the AT-rich DNA binding domain of Scm3^{HJURP} [30]. While we aim to further investigate this mechanism, either possibility yields a model of Scm3^{HJURP}-catalyzed Cse4^{CENP-A} nucleosome formation that is supported by *in vitro* reconstitutions, where it was found that Scm3^{HJURP} was required to form a Cse4^{CENP-A} nucleosome on the highly AT-rich (and thus inherently unfavorably for histone wrapping) centromeric DNA [30]. In addition, this is consistent with *in vivo* studies that showed Scm3^{HJURP} coordinates with Ndc10 to deposit Cse4^{CENP-A} at the centromere and is persistent at centromeres after Cse4^{CENP-A} deposition, although undergoing rapid exchange [30, 55].

A functional role for the essential centromere element CDEII

The single molecule TIRFM colocalization assays developed here enabled direct assessment of a functional role of the centromeric CDEII element, a question that has been extremely difficult to address *in vivo*. While there is no sequence conservation across CDEII elements in yeast, they are often among the highest A/T content loci within chromosomes [45]. This is a conserved feature across centromeres in both yeast and higher organisms despite being unfavorable for core histone wrapping [74]. Our work uncovered a role for CDEII sequence composition in stable Cse4^{CENP-A} nucleosome recruitment and suggests that A/T-run content contributes to stable incorporation of Cse4^{CENP-A}. The requirement for AT-run content for centromere function *in vivo* is highlighted by the failure of the canonical nucleosome targeting Widom 601-based centromere (Widom 601-hybrid), which contains little AT-run content, to stably recruit Cse4^{CENP-A} in our assay (Figure 6E), despite readily forming in reconstitutions [30]. This points to potential significant differences in the formation of native centromeric complexes and their recombinant counterparts. In addition, it remains an open question whether yeast CDEII element sequences have evolved to maximize

Cse4^{CENP-A} recruitment and stability or have evolved to a point where Cse4^{CENP-A} stability is sufficient to maintain centromere identity, as no A/T run beyond 8 nucleotides occurs within CDEII sequences despite occurring outside of centromeric loci [45]. In organisms with more complex centromeric architectures, high A/T-run content is not maintained which is why despite maintaining high A/T composition, they fail to substitute for CDEII function in yeast centromeres (Figure 6E). The reason for this lack of A/T-run content is not clear, but it may be a result of more complex regulatory schema for CENP-A targeting and deposition.

Our work also supports a previously proposed model where this AT-rich centromeric DNA also functions to restrict canonical histone formation, which in turn reduces Cse4^{CENP-A} stability [28, 30]. This model is consistent with findings in other organisms where H3 histone eviction was an inherent property of centromeric DNA [46] and with our own findings that H3 has low occupancy on the CEN3 templates [52] (Supp. Figure 7). This potential functional role of centromere sequence and/or centromere-binding kinetochore proteins in H3-eviction may be providing a drive to the genetic conservation of AT-rich DNA amongst centromere sequences. We speculate that in yeast, additional DNA-binding kinetochore proteins arose to aid in overcoming this kinetic barrier and to protect centromere function. This may be a consequence of the case that despite a lack of meiotic drive, yeast centromeres are among the fastest evolving regions of the yeast genome [75] and are thus sensitive to negative genetic drift resulting in complete loss of centromere identity. Rapid genetic drift may have also given rise to the accumulation of polymorphic A/T-run content within CDEII elements, which we found correlated to stable Cse4^{CENP-A} recruitment. This was somewhat unexpected, as homopolymeric repeats not only resist nucleosome formation [76], but they also tend to resist curvature [77]. However, the DNA bend at centromeres contributes to their stability in cells [78]. We therefore propose that polymorphic A/T-runs are cooperative with additional DNA-associated kinetochore proteins to facilitate nucleosome stability and kinetochore assembly and may explain the observed requirement for the A/T-rich DNA-binding Scm3^{HJURP} to catalyze centromeric DNA wrapping of Cse4^{CENP-A} (Figure 3, 4). The precise mechanism by which these A/T runs contribute to nucleosome formation remains open for further study, but at the very least may provide context for the required coordination of several DNA-binding proteins that are in close proximity to the Cse4^{CENP-A} nucleosome (Figure 7).

Taken together, our findings here provide further evidence of a robust intrinsic negative regulatory mechanism that prevents canonical H3-containing nucleosomes from forming stably at centromeric DNA, likely at the cost of inherent Cse4^{CENP-A} nucleosome stability. Only through coordination of centromeric DNA-binding proteins and the Scm3^{HJURP} chaperone can Cse4^{CENP-A} be efficiently targeted and maintained at the centromere and then further stabilized by subsequent DNA-interacting CCAN proteins. Once formed, this centromeric DNA complex provides a stable platform for subsequent kinetochore assembly and function (Figure 7). Adaptation of the assay developed here to study downstream kinetochore assembly is certainly possible and will enable the study of contributions of various kinetochore proteins from within the vast network required to form a functional kinetochore scaffold. This assay may also be adapted to study the dynamics of other histones and chaperones as well as to further recapitulate a native centromere "cell-like" environment by including processes such as centromere replication, which precludes kinetochore assembly in cells [52, 69, 72]. In addition, templates that include more complex chromatin structures surrounding the centromere that may provide additional information about the roles pericentromeric chromatin has in maintenance of centromere identity and

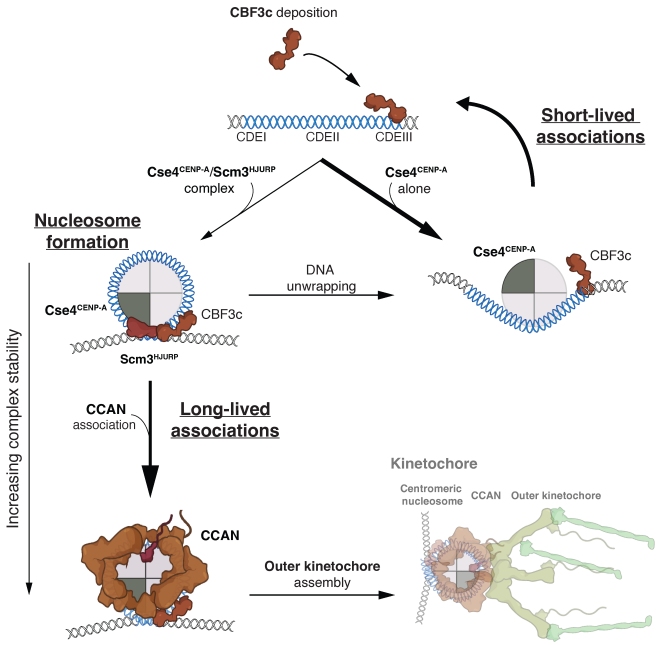

Figure 7. Formation of stable centromeric nucleosome requires tight coordination of centromeric DNA, Cse4^{CENP-A} with its chaperone Scm3^{HJURP} and subsequent CCAN kinetochore protein association. Schematic of centromeric nucleosome formation highlighting the different pathways that could lead to either short-lived or long-lived residences Cse4^{CENP-A} as measured in TIRFM resident lifetime assays.

function. Such adaptations may be needed to better understand how such an initially tenuous assembly pathway with stringent prerequisite conditions occurs so rapidly and with such fidelity in cells throughout passage of every cell cycle. The mechanisms that drive this process and that may be abrogated in various cellular disease states are a critical ongoing and future area of study.

Materials and Methods

Yeast Methods

The *S. cerevisiae* strains used in this study are listed in Supplemental Table 1 and are derivative of SBY3 (W303). Standard genetic crosses, media and microbial techniques were used. Cse4 was tagged internally at residue 80 with eGFP including linkers on either side (pSB1617) and then expressed from its native promoter at an exogenous locus in a *cse4Δ* background (SBY19926). Genes that were changed to include endogenously tagged fluorescent protein alleles (mCherry) or epitope tags (-13myc) or auxin-inducible degrons (-IAA7) were constructed at the endogenous loci by standard PCR-based integration techniques [79] and confirmed by PCR. The mutant *chl4-K13S* was made via PCR-based integration from a vector containing the *CHL4* gene with 13 mutations [45] present (pSB2182). The plasmids and primers used to generate strains are listed in Supplemental Tables 2 and 3, respectively. All liquid cultures were grown in yeast peptone dextrose rich (YPD) media. To arrest cells in mitosis, log phase cultures were diluted in liquid media to a final concentration of 30 µg/mL benomyl and grown for another three hours until at least 90% of cells were large-budded. For strains with auxin inducible degron (AID) alleles, all cultures used in the experiment were treated with 500 µM indole-3-acetic acid (IAA, dissolved in DMSO) for the final 60 min of growth (*scm3-AID*, *okp1-AID*) as described previously [53, 58, 80]. For strains with galactose inducible alleles (*pGAL*), cultures

were treated with 4% galactose for final 60 min of growth (*pGAL-PSH1*, *pGAL-SCM3*). Growth assays were performed by diluting log phase cultures to OD600 ~ 1.0 from which a 1:5 serial dilution series was made. This series was plated on YPD and YP plates that contained 4% galactose and incubated at 23℃.

Preparation of DNA templates, and Dynabeads

Plasmid pSB963 was used to generate the WT CEN3 DNA templates and pSB972 was used to generate the CEN3^{mut} template used in this study. Derivatives of pSB963 were altered using mutagenic primers and Q5 site-directed mutagenesis kit (NEB) to generate vectors containing CEN9, stable1, stable2, unstable1, unstable2, α-sat, and 80bp-CDEIII sequences (pSB3338, pSB3336, pSB3416, pSB3337, pSB3415 and pSB3335, respectively). CDEII mutants were taken directly from high-loss and low-loss pools from [45], where unstable1 is equivalent to H1, unstable2 is equivalent to H14, stable1 is equivalent to L1, and stable2 is equivalent to L5. Widom-601 template was equivalent to one used in structural studies [31] where CENIII (92-137) was inserted into corresponding region of 601 sequence (pSB3264). For α-sat CEN3 DNA, CDEII region of CEN3 template was mutated to a fragment of alpha-satellite DNA from *H. sapiens* X-chromosome based on structural studies containing CENP-A [36]. DNA templates were generated by PCR using a 5'-ATTO647-funtionalized (IDT DNA) 5' primer with homology to linker DNA upstream of ~60 bp of pericentromeric DNA and the centromere (SB7843) and a 5'-biotinylated (IDT DNA) 3' primer with linker DNA, an EcoRI restriction site, and homology to linker DNA downstream of ~ 60 bp of pericentromeric DNA and the centromere (SB3879) to yield ~750 bp dye-labeled assembly templates. For the 80 bp CDEIII mutant, plasmid pSB963 was amplified with primers SB7843 and SB7844 to generate CDEIII-containing mutant of 80bp total length. For CEN7, template pSB2953 was amplified with primers SB5699 and SB7842 to generate dye-labeled and biotinylated 750 bp assembly template. For double-tethered CEN3 DNA template, biotinylated primers SB7845 and SB3878 were used to 250 bp template, single-tethered 250 bp control template was generated using primers SB7846 and SB3878. Widom-601 template (pSB2887) and Widom-601-CDEIII hybrid template (pSB3264) were amplified with primers SB5699 and SB7842 to generate dye-labeled and biotinylated 750 bp templates. Supplemental Table 2 includes the plasmids used in this study and Supplemental Table 3 includes the primer sequences used to PCR amplify the DNA templates. PCR products were purified using the Qiagen PCR Purification Kit. In the case of bulk assembly for Mnase assays, purified CEN3 DNA was conjugated to Streptadivin-coated Dynabeads (M-280 Streptavidin, Invitrogen) for 2.5 hr at room temperature, using 1 M NaCl, 5 mM Tris-HCl (pH7.5), and 0.5 mM EDTA as the binding and washing buffer. For single molecule TIRFM assays, purified DNA was diluted in dH_2O to a final concentration ~100pM.

Whole Cell Extract preparation for kinetochore assembly assays

For a standard bulk kinetochore assembly assay *in vitro*, cells were grown in liquid YPD media to log phase and arrested in mitosis in 500 mL and then harvested by centrifugation. All subsequent steps were performed on ice with 4℃ buffers. Cells were washed once with dH2O with 0.2 mM PMSF, then once with Buffer L (25 mM HEPES pH 7.6, 2 mM MgCl2, 0.1 mM EDTA pH 7.6, 0.5 mM EGTA pH 7.6, 0.1 % NP-40, 175 mM K-Glutamate, and 15% Glycerol) supplemented with protease inhibitors (10 mg/ml leupeptin, 10mg/ml pepstatin, 10mg/ml chymostatin, 0.2 mM PMSF), and 2 mM DTT. Cell pellets were then snap frozen in liquid nitrogen and then lysed using a Freezer/Mill (SPEX SamplePrep), using 10 rounds that consisted of 2 min of bombarding the pellet at 10 cycles per second, then cooling for 2 min. The subsequent powder was weighed and then resuspended in Buffer L according to the following calculation: weight of pellet (g) x 2=number of mL of Buffer L. Resuspended cell lysate was thawed on ice and clarified by centrifugation at 16,100 g for 30 min at 4℃, protein-containing layer was extracted with a syringe, aliquoted and snap frozen in liquid nitrogen. The resulting soluble whole cell extracts (WCE) generally have a concentration of 50–70 mg/ml. The pellets, powder, and WCE were stored at -80℃.

Bulk assembly assays followed by Mnase treatment

De novo kinetochore assembly was performed with whole cell extract from SBY21110 (Ndc10-mCherry, Cse4-GFP) as previously described [53]. Briefly, 1 mL of whole cell extract and 50 µl of DNA coated M280 Dynabeads (single-tether CEN3, double-tether CEN3, or CEN3^{mut}) were incubated at room temperature for 90 min to allow kinetochore assembly. Following the final wash, beads were resuspended in 90 µL of Buffer L (see above) supplemented with 100 µg/mL BSA, 10 µL of 10X Micrococcal Nuclease Reaction Buffer (NEB) and 1000 gel units of Micrococcal Nuclease (NEB, #M0247S) and incubated at 30℃ for 10 min under constant mixing. Reaction was stopped with addition of EGTA to 10 mM. After removal of magnetic beads, aqueous phase was phenol-extracted followed by ethanol precipitation of DNA and resuspended in dH_20 and run on 1% agarose gel. Resolved DNA were visualized via SYBR Gold nucleic acid dye (Invitrogen; S11494) on ChemiDoc Imager (Bio-Rad).

Immunoblotting

For immunoblots, proteins were transferred from SDS-PAGE gels onto 0.22 µM cellulose paper, blocked at room temperature with 4% milk in PBST, and incubated overnight at 4 °C in primary antibody. Antibody origins and dilutions in PBST were as follows: α-Cse4 (9536 [81]; 1:500), α-H3 Alexa Fluor 555 (Invitrogen; 17H2L9; 1:3,000), α-PGK1 (Invitrogen; 4592560; 1:10,000). The anti-Scm3 antibodies were generated in rabbits against a recombinant Scm3 protein fragment (residues 1-28) of the protein by Genscript. The company provided affinity-purified antibodies that we validated by immunoprecipitating Scm3 from yeast strains with Scm3-V5 and confirming that the antibody recognized a protein of the correct molecular weight that was recognized by α-V5 antibody (Invitrogen; R96025; 1:5000). We subsequently used the antibody at a dilution of 1:10,000. Secondary antibodies were validated by the same methods as the primary antibodies as well as with negative controls lacking primary antibodies to confirm specificity. Blots were then washed again with PBST and incubated with secondary antibody at room temperature. Secondary antibodies were α-mouse (NA931) or α-rabbit (NA934), horseradish peroxidase-conjugated purchased from GE Healthcare and used at 1:1000 dilution in 4% milk in PBST. Blots were then washed again with PBST and ECL substrate from Thermo Scientific used to visualize the proteins on ChemiDoc Imager (Bio-Rad).

Single molecule TIRFM slide preparation

Coverslips and microscope slides were ultrasonically cleaned and passivated with PEG as described previously [82, 83]. Briefly, ultrasonically cleaned slides were treated with vectabond (Vector Laboratories) prior to incubation with 1% (w/v) biotinylated mPEG-SVA MW-5000K/mPEG-SVA MW-5000K (Lysan Bio) in flow chambers made with double-sided tape. Passivation was carried out overnight at 4℃. After passivation, flow chambers were washed with Buffer L and then incubated with 0.3 M BSA/0.3M Kappa Casein in Buffer L for 5 min. Flow chambers were washed with Buffer L and then incubated with 0.3 M Avidin DN (Vector Laboratories) for 5 min. Flow chambers were then washed with Buffer L and incubated with ~100 pM CEN3 DNA

template for 5 min and washed with Buffer L. For endpoint colocalization assays, slides were prepared as follows: Flow chambers were filled with 100 µL of WCE containing protein(s) of interest via pipetting and wicking with filter paper. After addition of WCE, slides were incubated for 90 min at 25°C and then WCE was washed away with Buffer L. Flow chambers were then filled with Buffer L with oxygen scavenger system [84] (10 nM PCD/2.5 mM PCA/1mM Trolox) for imaging. For immunofluorescence of H3, after 90 min, chambers were washed with Buffer L and then incubated for 30 min with Buffer L and 1:300 diluted antibody (Invitrogen 17H2L9). Chambers were then washed with Buffer L prior to imaging in Buffer L with oxygen scavenger system (above). For real-time colocalization assays, slides were prepared as follows: On the microscope, 100 µL WCE spiked with oxygen scavenger system was added to flow chamber via pipetting followed by immediate image acquisition.

Single molecule TIRFM colocalization assays image collection and analysis

All images were collected on a Nikon TE-2000 inverted TIRF microscope with a 100x oil immersion objective (Nikon Instruments) with an Andor iXon X3 EMCCD camera. Atto-647 labeled CEN3 DNAs were excited at 640 nm for 300 ms, GFP-tagged proteins were excited at 488 nm for 200 ms, and mCherry-tagged proteins were excited at 561 nm for 200 ms. For endpoint colocalization assays, single snapshots of all channels were acquired. For real-time colocalization assays images in 561 nm channel and 488 nm channel were acquired every 5 s with acquisition of the DNA-channel (647 nm) every 1 min for 45 min total (541 frames) using Nikon Elements acquisition software. Snapshots were processed in a CellProfiler 4 image analysis [85] pipeline using RelateObjects module to determine colocalization between DNA channel (647 nm) and GFP (488 nm) and mCherry (561 nm) channels. Results were quantified and plotted using MATLAB (The Mathworks, Natick, MA). Adjustments to example images (contrast, false color, etc.) were made using FIJI [86].

For real-time colocalization assay, a custom-built image analysis pipeline was built in MATLAB (R2019b) to extract DNA-bound intensity traces for the different fluorescent species, to convert them into ON/OFF pulses and to generate the empirical survivor function data. First, the image dataset was drift-corrected using either fast Fourier Transform cross-correlations or translation affine transformation depending on the severity of the drift. DNA spots were identified after binarizing the DNA signal using global background value as threshold, as well as size and time-persistency filtering. Mean values of z-normalized fluorescent markers intensities were measured at each DNA spot at each time frame, and local background was subtracted. Z-normalized traces were then binarized to ON/OFF pulses by applying a channel-specific, manually adjusted threshold value unique to all traces in a given image set. Pulses onsets, durations and overlaps between channels were then derived. Pulses in ON state at the beginning or the end of the recording were censored. For plotting clarity, z-normalized traces shown in the figures were zero-adjusted so that the baseline signal lies around zero. Kaplan Meyer analysis and log rank tests were performed in MATLAB (R2021a). Adjustments to example plot images (contrast) as well as generation of example plot source movies were made using FIJI [86].

Author Contributions and Notes

A.R.P conceptually designed and performed experiments, analyzed data, and wrote the manuscript with input from all authors; J.D.L. conceptually designed experiments and edited the manuscript. J.D. designed data analysis software and reviewed and edited the manuscript. C.L.A. and S.B. conceptually designed and supervised experiments and reviewed and edited the manuscript.

Statistics

P-values for comparing the Kaplan–Meier survival plots of Figure 4F, Figure 5F and Supp. Figure 5 D are provided in the legend and were computed using the log-rank test.

Data code and availability

Custom software written in MATLAB (R2021a) was used for TIRF colocalization residence lifetime analysis and plot generation. The source code is publicly available at https://github.com/FredHutch/Automated-Single-Molecule-Colocalization-Analysis. All data reported in this paper will be shared by the lead contact upon request.

The authors declare no conflict of interest.
This article contains supporting information online.

Acknowledgments

All imaging was performed at the Fred Hutchinson Cancer Center Cellular Imaging Core (supported by the Fred Hutch/University of Washington Cancer Consortium P30 CA015704), and we thank Jin Meng and Lena Schroeder for their experimental help. We also thank members of the S.B. and C.L.A. labs for critical reading of the manuscript. A.R.P. was supported by postdoctoral fellowship NIH F32GM136010. J.L. was supported by NIH CVP 5T32HL7312-39 and a fellowship from the Washington Research Foundation Fellowship Award. C.L.A. was supported by R01GM079373 and R35GM134842. S.B. was supported by NIH R01GM064386 and is also an investigator of the Howard Hughes Medical Institute.

References

1. Biggins, S., *The composition, functions, and regulation of the budding yeast kinetochore.* Genetics, 2013. **194**(4): p. 817-46.
2. Cheeseman, I.M., *The kinetochore.* Cold Spring Harb Perspect Biol, 2014. **6**(7): p. a015826.
3. Kixmoeller, K., P.K. Allu, and B.E. Black, *The centromere comes into focus: from CENP-A nucleosomes to kinetochore connections with the spindle.* Open Biol, 2020. **10**(6): p. 200051.
4. Musacchio, A. and A. Desai, *A molecular view of kinetochore assembly and function.* Biology (Basel), 2017. **6**(1).
5. Santaguida, S. and A. Musacchio, *The life and miracles of kinetochores.* EMBO J, 2009. **28**(17): p. 2511-31.
6. Gordon, D.J., B. Resio, and D. Pellman, *Causes and consequences of aneuploidy in cancer.* Nat Rev Genet, 2012. **13**(3): p. 189-203.
7. Herman, J.A., et al., *Molecular pathways: regulation and targeting of kinetochore-microtubule attachment in cancer.* Clin Cancer Res, 2015. **21**(2): p. 233-9.
8. Holland, A.J. and D.W. Cleveland, *Boveri revisited: chromosomal instability, aneuploidy and tumorigenesis.* Nat Rev Mol Cell Biol, 2009. **10**(7): p. 478-87.
9. Sheltzer, J.M., et al., *Aneuploidy drives genomic instability in yeast.* Science, 2011. **333**(6045): p. 1026-30.
10. Clarke, L. and J. Carbon, *The structure and function of yeast centromeres.* Annu Rev Genet, 1985. **19**.
11. Cleveland, D.W., Y. Mao, and K.F. Sullivan, *Centromeres and kinetochores: from epigenetics to mitotic checkpoint signaling.* Cell, 2003. **112**(4): p. 407-21.
12. McAinsh, A.D. and A.L. Marston, *The four causes: The functional architecture of centromeres and kinetochores.* Annu Rev Genet, 2022. **56**: p. 279-314.
13. Palmer, D.K., et al., *Purification of the centromere-specific protein CENP-A and demonstration that it is a distinctive histone.* Proc Natl Acad Sci U S A, 1991. **88**(9): p. 3734-8.

14. Sullivan, K.F., M. Hechenberger, and K. Masri, *Human CENP-A contains a histone H3 related histone fold domain that is required for targeting to the centromere.* J Cell Biol, 1994. **127**(3): p. 581-92.
15. Camahort, R., et al., *Scm3 is essential to recruit the histone H3 variant cse4 to centromeres and to maintain a functional kinetochore.* Mol Cell, 2007. **26**(6): p. 853-65.
16. Dunleavy, E.M., et al., *HJURP is a cell-cycle-dependent maintenance and deposition factor of CENP-A at centromeres.* Cell, 2009. **137**(3): p. 485-97.
17. Foltz, D.R., et al., *Centromere-specific assembly of CENP-A nucleosomes is mediated by HJURP.* Cell, 2009. **137**(3): p. 472-84.
18. Mizuguchi, G., et al., *Nonhistone Scm3 and histones CenH3-H4 assemble the core of centromere-specific nucleosomes.* Cell, 2007. **129**(6): p. 1153-64.
19. Stoler, S., et al., *Scm3, an essential Saccharomyces cerevisiae centromere protein required for G2/M progression and Cse4 localization.* Proc Natl Acad Sci U S A, 2007. **104**(25): p. 10571-6.
20. McKinley, K.L. and I.M. Cheeseman, *The molecular basis for centromere identity and function.* Nat Rev Mol Cell Biol, 2016. **17**(1): p. 16-29.
21. Shrestha, R.L., et al., *Mislocalization of centromeric histone H3 variant CENP-A contributes to chromosomal instability (CIN) in human cells.* Oncotarget, 2017. **8**(29): p. 46781-46800.
22. Filipescu, D., et al., *Essential role for centromeric factors following p53 loss and oncogenic transformation.* Genes Dev, 2017. **31**(5): p. 463-480.
23. Mahlke, M.A. and Y. Nechemia-Arbely, *Guarding the genome: CENP-A-chromatin in health and cancer.* Genes (Basel), 2020. **11**(7).
24. Kunkel, G.R. and H.G. Martinson, *Nucleosomes will not form on double-stranded RNa or over poly(dA).poly(dT) tracts in recombinant DNA.* Nucleic Acids Res, 1981. **9**(24): p. 6869-88.
25. Prunell, A., *Nucleosome reconstitution on plasmid-inserted poly(dA) . poly(dT).* EMBO J, 1982. **1**(2): p. 173-9.
26. Dechassa, M.L., K. Wyns, and K. Luger, *Scm3 deposits a (Cse4-H4)2 tetramer onto DNA through a Cse4-H4 dimer intermediate.* Nucleic Acids Res, 2014. **42**(9): p. 5532-42.
27. Dechassa, M.L., et al., *Structure and Scm3-mediated assembly of budding yeast centromeric nucleosomes.* Nat Commun, 2011. **2**: p. 313.
28. Xiao, H., et al., *Nonhistone Scm3 binds to AT-rich DNA to organize atypical centromeric nucleosome of budding yeast.* Mol Cell, 2011. **43**(3): p. 369-80.
29. Guan, R., et al., *Structural and dynamic mechanisms of CBF3-guided centromeric nucleosome formation.* Nat Commun, 2021. **12**(1): p. 1763.
30. Zhou, B.R., et al., *Atomic resolution cryo-EM structure of a native-like CENP-A nucleosome aided by an antibody fragment.* Nat Commun, 2019. **10**(1): p. 2301.
31. Lowary, P.T. and J. Widom, *New DNA sequence rules for high affinity binding to histone octamer and sequence-directed nucleosome positioning.* J Mol Biol, 1998. **276**(1): p. 19-42.
32. Yan, K., et al., *Architecture of the CBF3-centromere complex of the budding yeast kinetochore.* Nat Struct Mol Biol, 2018. **25**(12): p. 1103-1110.
33. Dendooven, T., et al., *Cryo-Em structure of the complete inner kinetochore of the budding yeast point centromere.* BioRxiv, 2022.
34. Yatskevich, S., et al., *Structure of the human inner kinetochore bound to a centromeric CENP-A nucleosome.* Science, 2022. **376**(6595): p. 844-852.
35. Carbon, J., *Yeast centromeres: structure and function.* Cell, 1984. **37**(2): p. 351-3.
36. Carbon, J. and L. Clarke, *Structural and functional analysis of a yeast centromere (CEN3).* J Cell Sci Suppl, 1984. **1**.
37. Cai, M. and R.W. Davis, *Yeast centromere binding protein CBF1, of the helix-loop-helix protein family, is required for chromosome stability and methionine prototrophy.* Cell, 1990. **61**: p. 437-446.
38. Hedouin, S., et al., *A transcriptional roadblock protects yeast centromeres.* Nucleic Acids Res, 2022. **50**(14): p. 7801-7815.
39. Cho, U.S. and S.C. Harrison, *Recognition of the centromere-specific histone Cse4 by the chaperone Scm3.* Proc Natl Acad Sci U S A, 2011. **108**(23): p. 9367-71.
40. Cole, H.A., B.H. Howard, and D.J. Clark, *The centromeric nucleosome of budding yeast is perfectly positioned and covers the entire centromere.* Proc Natl Acad Sci U S A, 2011. **108**(31): p. 12687-92.
41. Cumberledge, S. and J. Carbon, *Mutational analysis of meiotic and mitotic centromere function in Saccharomyces cerevisiae.* Genetics, 1987. **117**(2): p. 203-12.
42. Gaudet, A. and M. Fitzgerald-Hayes, *Alterations in the adenine-plus-thymine-rich region of CEN3 affect centromere function in Saccharomyces cerevisiae.* Mol Cell Biol, 1987. **7**(1): p. 68-75.
43. Baker, R.E. and K. Rogers, *Genetic and Genomic Analysis of the AT-Rich Centromere DNA Element II of S. cerevisiae.* Genetics, 2005.
44. Shukla, M., et al., *Centromere DNA destabilizes H3 nucleosomes to promote CENP-A deposition during the cell cycle.* Curr Biol, 2018. **28**(24): p. 3924-3936 e4.
45. Yan, K., et al., *Structure of the inner kinetochore CCAN complex assembled onto a centromeric nucleosome.* Nature, 2019. **574**(7777): p. 278-282.
46. Dhatchinamoorthy, K., et al., *Structural plasticity of the living kinetochore.* J Cell Biol, 2017. **216**(11): p. 3551-3570.
47. Joglekar, A.P., et al., *Molecular architecture of a kinetochore-microtubule attachment site.* Nat Cell Biol, 2006. **8**(6): p. 581-5.
48. Friedman, L.J., J. Chung, and J. Gelles, *Viewing dynamic assembly of molecular complexes by multi-wavelength single-molecule fluorescence.* Biophys J, 2006. **91**(3): p. 1023-31.
49. Friedman, L.J. and J. Gelles, *Mechanism of transcription initiation at an activator-dependent promoter defined by single-molecule observation.* Cell, 2012. **148**(4): p. 679-89.
50. Hoskins, A.A., et al., *Ordered and dynamic assembly of single spliceosomes.* Science, 2011. **331**(6022): p. 1289-95.
51. Furuyama, S. and S. Biggins, *Centromere identity is specified by a single centromeric nucleosome in budding yeast.* Proc Natl Acad Sci U S A, 2007. **104**(37): p. 14706-11.
52. Lang, J., A. Barber, and S. Biggins, *An assay for de novo kinetochore assembly reveals a key role for the CENP-T pathway in budding yeast.* Elife, 2018. **7**.
53. Crawford, D.J., et al., *Visualizing the splicing of single pre-mRNA molecules in whole cell extract.* RNA, 2008. **14**(1): p. 170-9.
54. Wisniewski, J., et al., *Imaging the fate of histone Cse4 reveals de novo replacement in S phase and subsequent stable residence at centromeres.* Elife, 2014. **3**: p. e02203.
55. McGrew, J., B. Diehl, and M. Fitzgerald-Hayes, *Single base-pair mutations in centromere element III cause aberrant chromosome segregation in Saccharomyces cerevisiae.* Mol Cell Biol, 1986. **6**(2): p. 530-8.
56. Cho, U.S. and S.C. Harrison, *Ndc10 is a platform for inner kinetochore assembly in budding yeast.* Nat Struct Mol Biol, 2011. **19**(1): p. 48-55.
57. Nishimura, K., et al., *An auxin-based degron system for the rapid depletion of proteins in nonplant cells.* Nat Methods, 2009. **6**(12): p. 917-22.
58. Popchock, A.R., et al., *Engineering heterodimeric kinesins through genetic incorporation of noncanonical amino acids.* ACS Chem Biol, 2018. **13**(8): p. 2229-2236.
59. Popchock, A.R., et al., *The mitotic kinesin-14 KlpA contains a context-dependent directionality switch.* Nat Commun, 2017. **8**: p. 13999.
60. Leber, V., A. Nans, and M.R. Singleton, *Structural basis for assembly of the CBF3 kinetochore complex.* EMBO J, 2018. **37**(2): p. 269-281.
61. Aravamudhan, P., I. Felzer-Kim, and A.P. Joglekar, *The budding yeast point centromere associates with two Cse4 molecules during mitosis.* Curr Biol, 2013. **23**(9): p. 770-4.
62. Collins, K.A., et al., *The overexpression of a Saccharomyces cerevisiae centromeric histone H3 variant mutant protein leads to a defect in kinetochore biorientation.* Genetics, 2007. **175**(2): p. 513-25.

63. Zhou, N., et al., *Molecular basis for the selective recognition and ubiquitination of centromeric histone H3 by yeast E3 ligase Psh1.* J Genet Genomics, 2021. **48**(6): p. 463-472.
64. Furuyama, T. and S. Henikoff, *Centromeric nucleosomes induce positive DNA supercoils.* Cell, 2009. **138**(1): p. 104-13.
65. Guo, M.S., et al., *High-resolution, genome-wide mapping of positive supercoiling in chromosomes.* Elife, 2021. **10**.
66. Hornung, P., et al., *A cooperative mechanism drives budding yeast kinetochore assembly downstream of CENP-A.* J Cell Biol, 2014. **206**(4): p. 509-24.
67. Hinshaw, S.M. and S.C. Harrison, *The structure of the Ctf19c/CCAN from budding yeast.* Elife, 2019. **8**.
68. Joglekar, A.P., et al., *Molecular architecture of the kinetochore-microtubule attachment site is conserved between point and regional centromeres.* J Cell Biol, 2008. **181**(4): p. 587-94.
69. Bobkov, G.O.M., et al., *Spt6 is a maintenance factor for centromeric CENP-A.* Nat Commun, 2020. **11**(1): p. 2919.
70. Hewawasam, G.S., et al., *Chromatin assembly factor-1 (CAF-1) chaperone regulates Cse4 deposition into chromatin in budding yeast.* Nucleic Acids Res, 2018. **46**(9): p. 4440-4455.
71. Lacoste, N., et al., *Mislocalization of the centromeric histone variant CenH3/CENP-A in human cells depends on the chaperone DAXX.* Mol Cell, 2014. **53**(4): p. 631-44.
72. Gkikopoulos, T., et al., *The SWI/SNF complex acts to constrain distribution of the centromeric histone variant Cse4.* EMBO J, 2011. **30**(10): p. 1919-27.
73. Ranjitkar, P., Press, M. O., Yi, X., Baker, R., MacCoss, M. J, Biggins, S, *An E3 ubiquitin ligase prevents ectopic localization of the centromeric histone H3 variant via the centromere targeting domain.* Mol Cell, 2010. **40**(3): p. 455-64.
74. Struhl, K. and E. Segal, *Determinants of nucleosome positioning.* Nat Struct Mol Biol, 2013. **20**(3): p. 267-73.
75. Bensasson, D., et al., *Rapid evolution of yeast centromeres in the absence of drive.* Genetics, 2008. **178**(4): p. 2161-7.
76. Liebl, K. and M. Zacharias, *Accurate modeling of DNA conformational flexibility by a multivariate Ising model.* Proc Natl Acad Sci U S A, 2021. **118**(15).
77. Drew, H.R. and A.A. Travers, *DNA bending and its relation to nucleosome positioning.* J Mol Biol, 1985. **186**(4): p. 773-90.
78. Murphy, M.R., D.M. Fowlkes, and M. Fitzgerald-Hayes, *Analysis of centromere function in Saccharomyces cerevisiae using synthetic centromere mutants.* Chromosoma, 1991. **101**(3): p. 189-97.
79. Longtine, M.S., et al., *Additional modules for versatile and economical PCR-based gene deletion and modification in Saccharomyces cerevisiae.* Yeast, 1998. **14**(10): p. 953-61.
80. Miller, M.P., C.L. Asbury, and S. Biggins, *A TOG protein confers tension sensitivity to kinetochore-microtubule attachments.* Cell, 2016. **165**(6): p. 1428-1439.
81. Pinsky, B.A., et al., *An Mtw1 complex promotes kinetochore biorientation that is monitored by the Ipl1/Aurora protein kinase.* Dev Cell, 2003. **5**(5): p. 735-45.
82. Larson, J.D., M.L. Rodgers, and A.A. Hoskins, *Visualizing cellular machines with colocalization single molecule microscopy.* Chem Soc Rev, 2014. **43**(4): p. 1189-200.
83. Larson, J.D. and A.A. Hoskins, *Dynamics and consequences of spliceosome E complex formation.* Elife, 2017. **6**.
84. Aitken, C.E., R.A. Marshall, and J.D. Puglisi, *An oxygen scavenging system for improvement of dye stability in single-molecule fluorescence experiments.* Biophys J, 2008. **94**(5): p. 1826-35.
85. Stirling, D.R., et al., *CellProfiler 4: improvements in speed, utility and usability.* BMC Bioinformatics, 2021. **22**(1): p. 433.
86. Schindelin, J., et al., *Fiji: an open-source platform for biological-image analysis.* Nat Methods, 2012. **9**(7): p. 676-82.
87. Sehnal, D., et al., *Mol* Viewer: modern web app for 3D visualization and analysis of large biomolecular structures.* Nucleic Acids Res, 2021. **49**(W1): p. W431-W437.